Integrated Geophysical Investigation to Delineate Deep Structural Features - A Case Study from the Eastern Part of Junggar Basin, NW China

Chunguan Zhang[1, 2]

[1]School of Earth Sciences and Engineering, Xi'an Shiyou University, Xi'an, China

[2]Shaanxi Key Laboratory of Petroleum Accumulation Geology, Xi'an Shiyou University, Xi'an, China

Email address:

chunguan-zhang@163.com

Abstract: In order to study the features of geophysical field and deep structure of the eastern part of Junggar basin, we collected gravity and magnetic data with a scale of 1:1,000,000. Then, we calculated the isostatic gravity anomaly based on the Bouguer gravity anomaly data and the aeromagnetic anomaly by reduction to the pole (RTP) based on the aeromagnetic anomaly data, separated the gravity anomalies and the magnetic anomalies using the filtering method and the wavelet transform method, and obtained the regional gravity and magnetic anomalies and the multi-order wavelet transform approximation of gravity and magnetic anomalies. Combined with existing geological and geophysical research, we analyzed the features of the gravity anomalies and the magnetic anomalies, and discussed the deep structure of the eastern part of Junggar basin. The results showed that the upper mantle uplift in the eastern part of Junggar basin. The Junggar basin turned down under the northern Tianshan orogenic belt and the eastern Junggar orogenic belt. The regional high gravity anomaly, high magnetic anomaly and high resistivity anomaly in the northern part of the eastern part of Junggar basin may be mainly caused by the influx of larger density, stronger magnetic property and larger resistivity mantle substances into the middle crust along the fault in the northern margin of the Junggar basin.

Keywords: Deep Structure, Integrated Geophysical Investigation, Gravity and Magnetic Anomalies, Eastern Part of Junggar Basin, NW China

1. Introduction

Xinjiang, located in the northwestern part of China, displays the style of Basin-Range tectonics. As a part of Xinjiang, there is a close relationship between the deep structural features and the distribution of the geophysical field. The predecessors have done a lot of work in the formation and evolution of the crust [1-5], and the previous researches have discussed the nature of the basement from different perspectives [6-10], but there are still opposing views for understanding the nature of the Junggar basin basement [10-12]. The studies on the nature of the basin basement and kinetic mechanism of crustal formation and evolution are inseparable from the information of the deep crustal structure. The predecessors have been used a variety of geophysical data to study the deep crustal structure, such as seismic tomography [13-15], deep seismic sounding [16, 17], regional gravity and magnetic data [18-21], satellite magnetic data [22], satellite gravity data [23, 24], and magnetotelluric sounding [25-27]. Although there are a variety of geophysical data, most researches are mainly based on a certain kind of geophysical data, and the studies on integrated geophysical data are relatively weak.

To discuss the deep geological significance of regional gravity and magnetic anomalies, in 2010, we collected gravity and magnetic data with a scale of 1:1,000,000. This paper, through separating the gravity and magnetic anomalies, analyzes the features of the Bouguer gravity anomaly, the isostatic gravity anomaly, the RTP aeromagnetic anomaly, the multiple-scale regional gravity

and magnetic anomalies, and the multi-order wavelet transform approximation of gravity and magnetic anomalies. Combined with the previous researches of the deep seismic sounding, magnetotelluric deep sounding, and deep geological, this paper is to discuss the deep geological genesis of the gravity and magnetic anomalies and the deep structure in the eastern part of Junggar basin.

2. Geologic Setting

The study area is located between 87.7° to 92°E and 43.4° to 45.8°N and covers an area of 84,000 km^2. The topographic map (Figure 1) shows that the area composes: a mountainous region in the Bogda-Danangou-Xialaoba area, a lowland in the Wucaiwan-Hangou area, and a hill country in the Kamusite-Suji area.
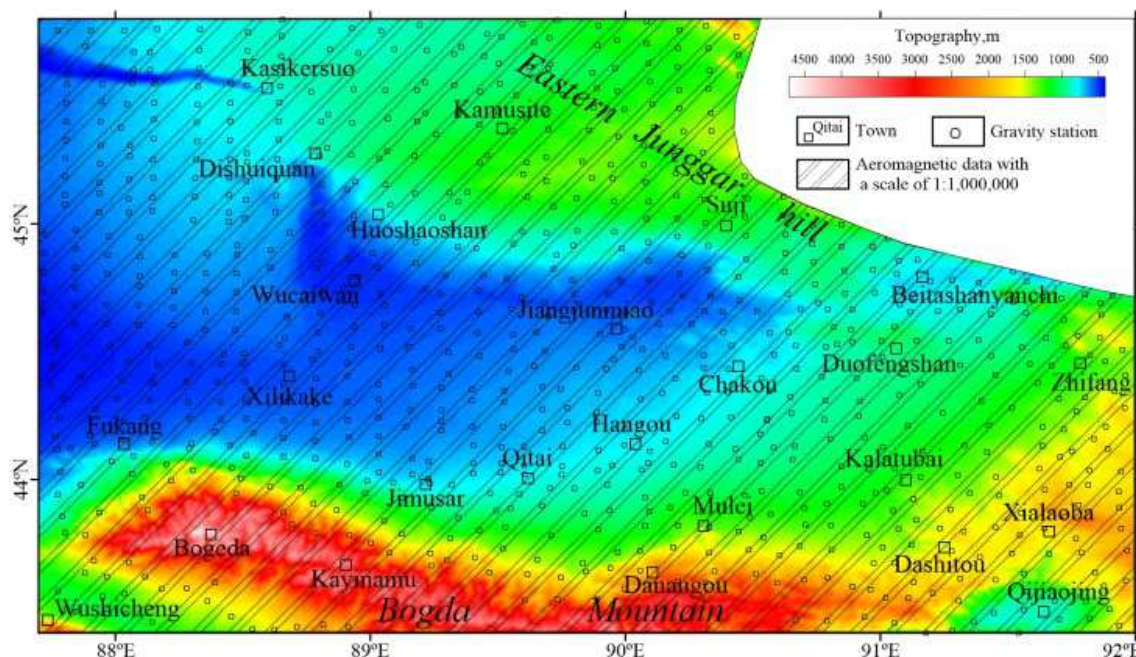
Figure 1. *Topographic map with distribution of gravity and aeromagnetic data in the eastern part of Junggar basin. The topography data derived from STRM30_PLUS V11, which was released by Scrpps institution of Oceanography, USA [28].*
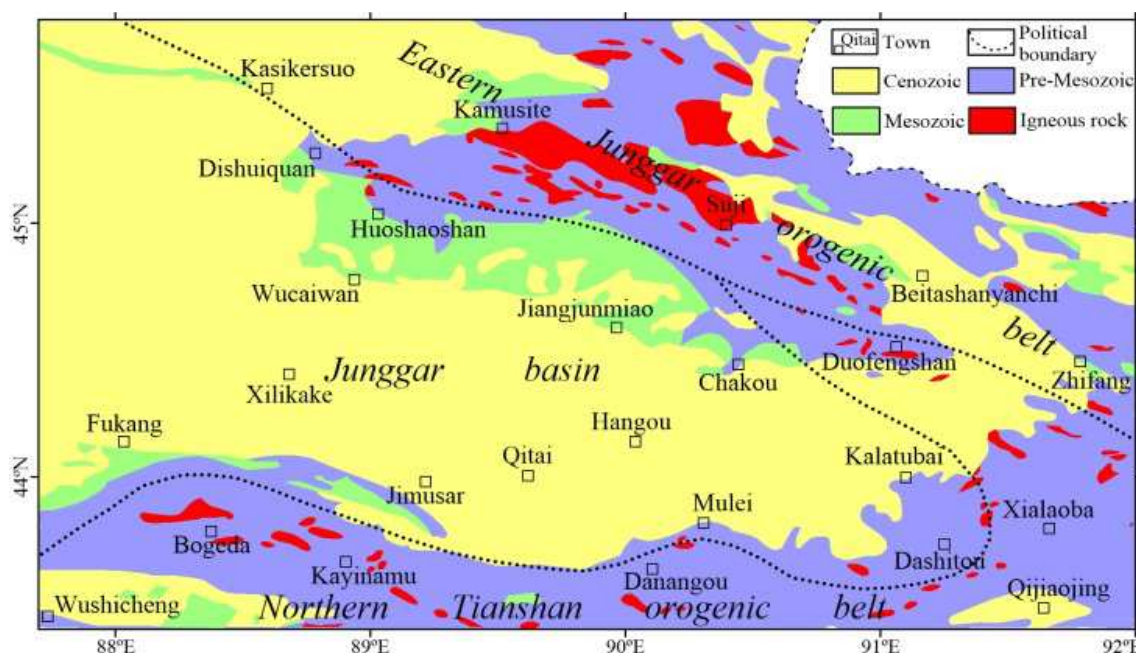
Figure 2. *Regional geologic map of the eastern part of Junggar basin.*

The study area consists primarily of three tectonic units, from south to north (Figure 2): the northern Tianshan orogenic belt, the Junggar basin, and the eastern Junggar orogenic belt

[19, 29]. Due to the Variscan orogeny, the prototypes of these basins formed. Then, the sedimentation continued to strengthen in the Middle-Late Carboniferous, and the

magmatic activity was intense. The geological map (Figure 2) shows that magmatic rocks are developed in this area. The acidic rocks are widely distributed in the Kamusite-Beitashanyanchi area of the eastern Junggar orogenic belt, and the intermediate rocks are scattered in the northern Tianshan orogenic belt. Spreading with pinch-and-swell form, the basic rocks are mainly distributed in the northern Tianshan orogenic belt, while the ultrabasic rocks are only found in the southwestern part of the eastern Junggar orogenic belt and are distributed in a band.

The sedimentary formations are widely developed throughout the study area, including the Cenozoic strata, the Mesozoic strata, and the Paleozoic strata (Figure 2). The Cenozoic strata are mainly distributed in the Junggar basin, and there are also low-lying areas in the eastern Junggar orogenic belt and the northern Tianshan orogenic belt. The Mesozoic strata are mainly distributed in the Wucaiwan-Chakou area and the Fukang-Jimusar area of the Junggar basin, and there are also small areas in the lower terrain areas of the eastern Junggar orogenic belt and the northern Tianshan orogenic belt. The Paleozoic strata are mainly distributed in the eastern Junggar orogenic belt and northern Tianshan orogenic belt, and there are also small areas in the northern and southern margins of the Junggar basin.

3. Data Acquisition and Interpretation

3.1. Data Acquisition

We collected gravity anomaly and aeromagnetic anomaly data with a scale of 1:1,000,000 in the study area, and the distribution of the gravity and aeromagnetic data shows in Figure 1. These gravity and aeromagnetic data arranged by Xi'an Center of Geological Survey of China Geological Survey in 2010. The gravity data includes 866 gravity stations, while the aeromagnetic data is a gridded data.

In order to further analyze the geological implications of the gravity anomalies and the magnetic anomalies, we also collected the deep seismic sounding data and the magnetotelluric deep sounding data, their distribution shown in Figure 3. The data of the deep seismic sounding is a profile with 371 km length, and this profile is coincident with a geoscience transect from Altay to Altun Tagh in the study area [16]. Based on the distribution direction, the profile of the deep seismic sounding includes two sections, the AB section and the BC section, and the AB section of the AC profile displays NS-trending and the BC section of the AC profile displays NWW-trending (Figure 3). The data of the magnetotelluric deep sounding is a high-resistivity distribution with 30 km depth [25].
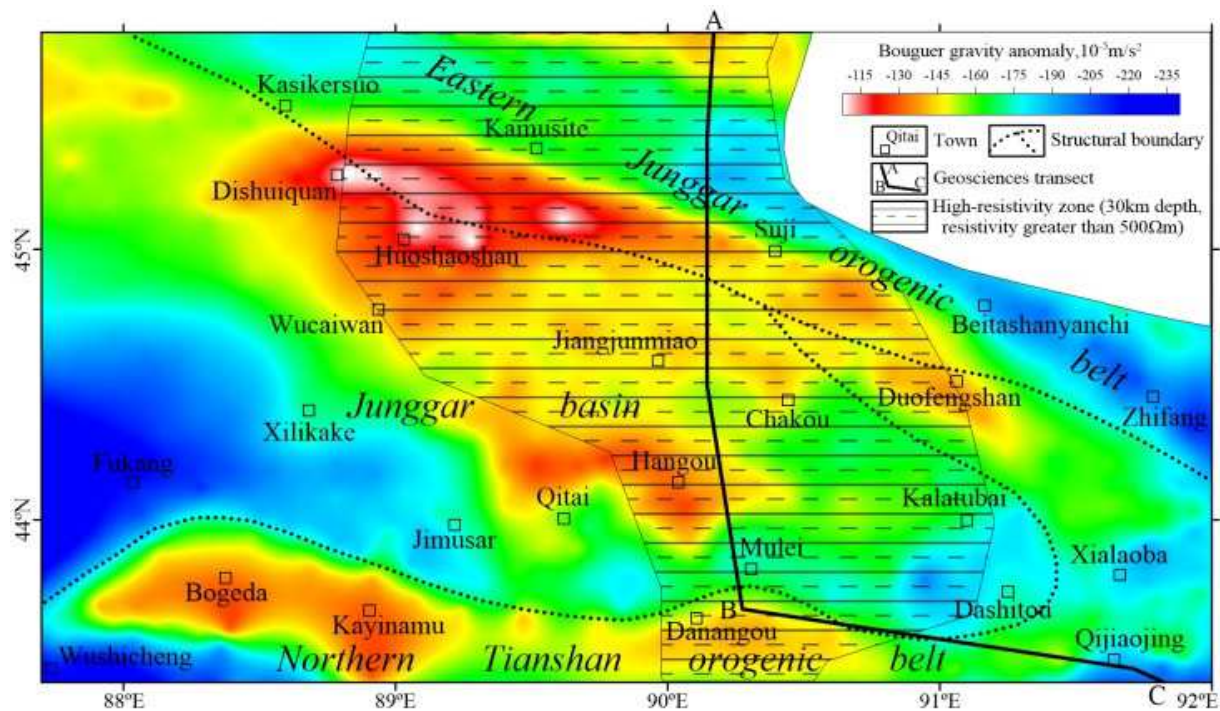
Figure 3. *Bouguer gravity anomaly map of the eastern part of Junggar basin (tectonic boundary modified after Li et al. (2007) [30], resistivity data modified after Li (1996) [25], geoscience transect data modified after Wang et al. (2004) [16]).*

3.2. Features and Geological Implication of the Gravity Anomalies

The Bouguer gravity anomaly map (Figure 3) shows that the gravity anomaly is characterized with clear zoning. In the northern Tianshan orogenic belt, the Bouguer gravity anomaly displays an EW-trending gravity high and a maximum value of -130×10^{-5}m/s^2 occurs in the south of Bogda. In the eastern Junggar orogenic belt, the Bouguer gravity anomaly displays an obvious NW-elongated gravity low occurs to the Kamusite-Zhifan area and on both northeast and southwest sides of the gravity low, two gravity highs are developed in parallel. In the Junggar basin, the Bouguer gravity anomalies

are clearly divided into a western area of gravity low and an eastern area of gravity high. The gradient of gravity anomaly changes obviously in the north side of the northern Tianshan orogenic belt, and the surface geological map displays the surface outcroppings that are mainly the transition zone from the Paleozoic strata to the Mesozoic-Cenozoic strata. These features suggest that the discordogenic fault developed in the north side of the northern Tianshan orogenic belt and controlled the development of the structural units. The gradient of gravity anomaly also changes obviously in the Kamusite-Suji-Zhifan area of the eastern Junggar orogenic belt, and the surface geological map displays the surface outcroppings that are mainly the acidic rocks with a large area. These features suggest that there is a fault zone in the Kamusite-Suji-Zhifan area of the eastern Junggar orogenic belt and the southern boundary of this fault zone is a tectonic boundary of the Junggar basin. The Bouguer gravity anomaly displays gravity high with a large area in the Dishuiquan-Hangou area of the Junggar basin, and the surface geological map displays the surface outcroppings that are mainly the Cenozoic strata with lower density. These features suggest that the high value of gravity anomaly is apparently controlled by the deep geological factors, and the depth of the substance with larger density is shallower in the eastern Junggar basin than in the west of the study area. That is to say, the composite density of the crust and upper mantle in the Dishuiquan-Hangou area is greater than that in the Fukang-Xilikake area of the Junggar basin.
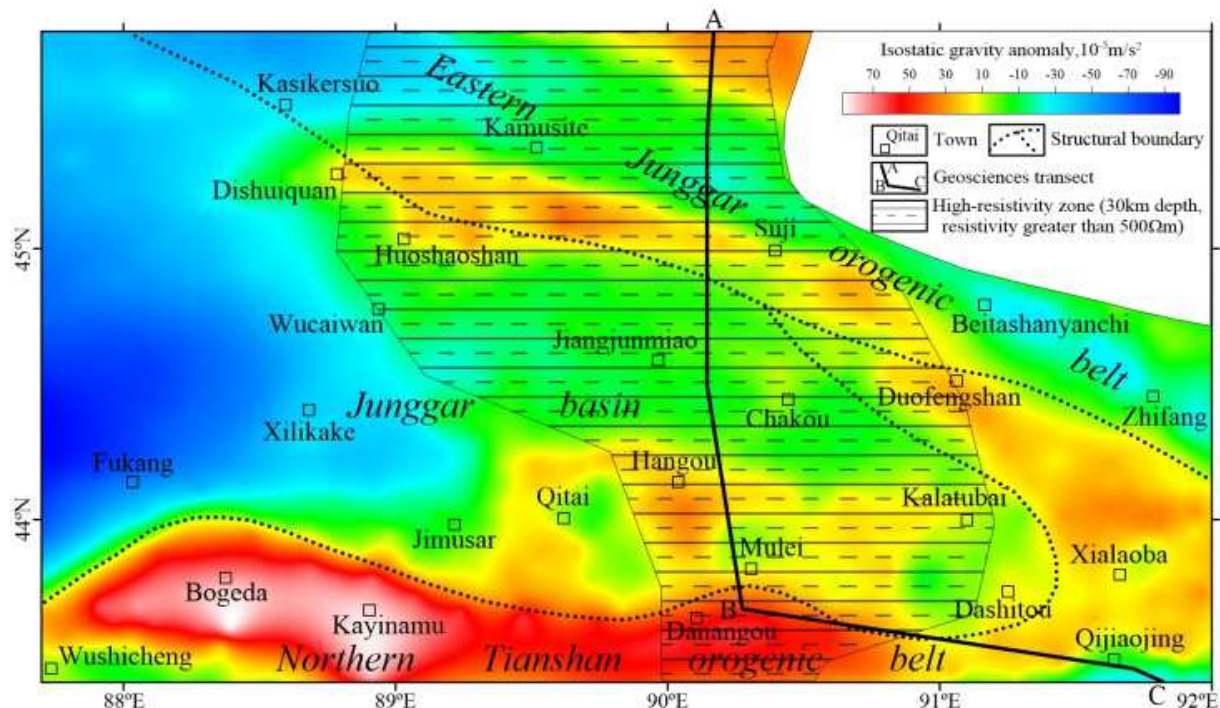

Figure 4. Isostatic gravity anomaly map of the eastern part of Junggar basin.

According to the previous researches of the Moho surface [31, 32], we selected a depth of 45 km as the average depth of the Moho surface in the study area. Based on the Airy equilibrium model and terrain elevation data with a $0.02° \times 0.02°$ grid, we used the Bouguer gravity anomaly data to calculate the isostatic gravity anomaly data. The isostatic gravity anomaly map (Figure 4) shows that the gravity values change obviously and a maximum value of $87 \times 10^{-5} m/s^2$ occurs in the south of Bogda and a minimum value of $-98 \times 10^{-5} m/s^2$ occurs in the west of Fukang. In the northern Tianshan orogenic belt, the isostatic gravity anomaly displays an EW-trending gravity high and an obvious gravity gradient, indicating that the crust is in non-equilibrium state and the compensation of the deep substance is serious surplus in this area. In the eastern Junggar orogenic belt, the features of the isostatic gravity anomaly is similar to that of the Bouguer gravity anomaly, but the isostatic gravity anomaly is relatively gentle, indicating that the crust is in non-equilibrium state and the compensation of the deep substance is still inadequate in this area. In the Junggar basin, the isostatic gravity anomaly is clearly divided into a western area of gravity low and an eastern area of gravity high. The isostatic gravity anomaly displays a low-value zone to the west of the Dishuiquan-Jimusar area, indicating that the crust is in non-equilibrium state and the compensation of the deep substance is serious shortage in this area. To the east of the Dishuiquan-Jimusar area, the isostatic gravity anomaly displays a macro high-value zone, while it is characterized with clear zoning from the north to the south. The isostatic gravity anomaly displays a relative low-value zone in the Wucaiwan-Chakou area, indicating that the crust is in non-equilibrium state and the compensation of the deep substance is slightly shortage in this area. The isostatic gravity anomaly displays a relative high-value zone in the Qitai-Kalatubai area, indicating that the crust is in non-equilibrium state and the compensation of the deep

substance is slightly surplus in this area.

The regional gravity anomalies are able to reflect the effects of the gravitational field induced by the large scale geological body. Suppressed the local anomalies and improved the resolving ability of the regional anomalies, the regional gravity anomalies can be accurately extracted. In order to obtain the regional gravity anomalies, the moving average method and the filter method are often applied [19, 33]. In this paper, the gravity anomalies were separated by the filtering technique [34]. Based on the Bouguer gravity anomaly data, we extracted the regional gravity anomalies with multi-filter scales of 30 km, 50 km, 80 km, and 120 km. The regional gravity anomaly map (Figure 5) shows that the gravity anomalies with a relatively small scale are suppressed with the filter window length increasing. The regional gravity anomalies with multi-filter scales of 30 km, 50 km, and 80 km

can reflect the rough sketch of the northern Tianshan orogenic belt, but the regional gravity anomalies with filter scale of 120 km cannot reflect this feature. These features suggest that the lateral density variation of the relatively shallower substance is obvious in the transition zone between the northern Tianshan orogenic belt and the Junggar basin, and the lateral density variation of the relatively deeper substance is indistinct in this area. There is a better relationship between the high-value zone of the regional gravity anomaly and the resistivity anomaly in the eastern part of the Junggar basin, especially the regional gravity anomaly with scale of 120 km. These features suggest that the lateral density variation of the deep substance with the depth greater than 30 km is small in the transition zone between the northern Tianshan orogenic belt and the Junggar basin.
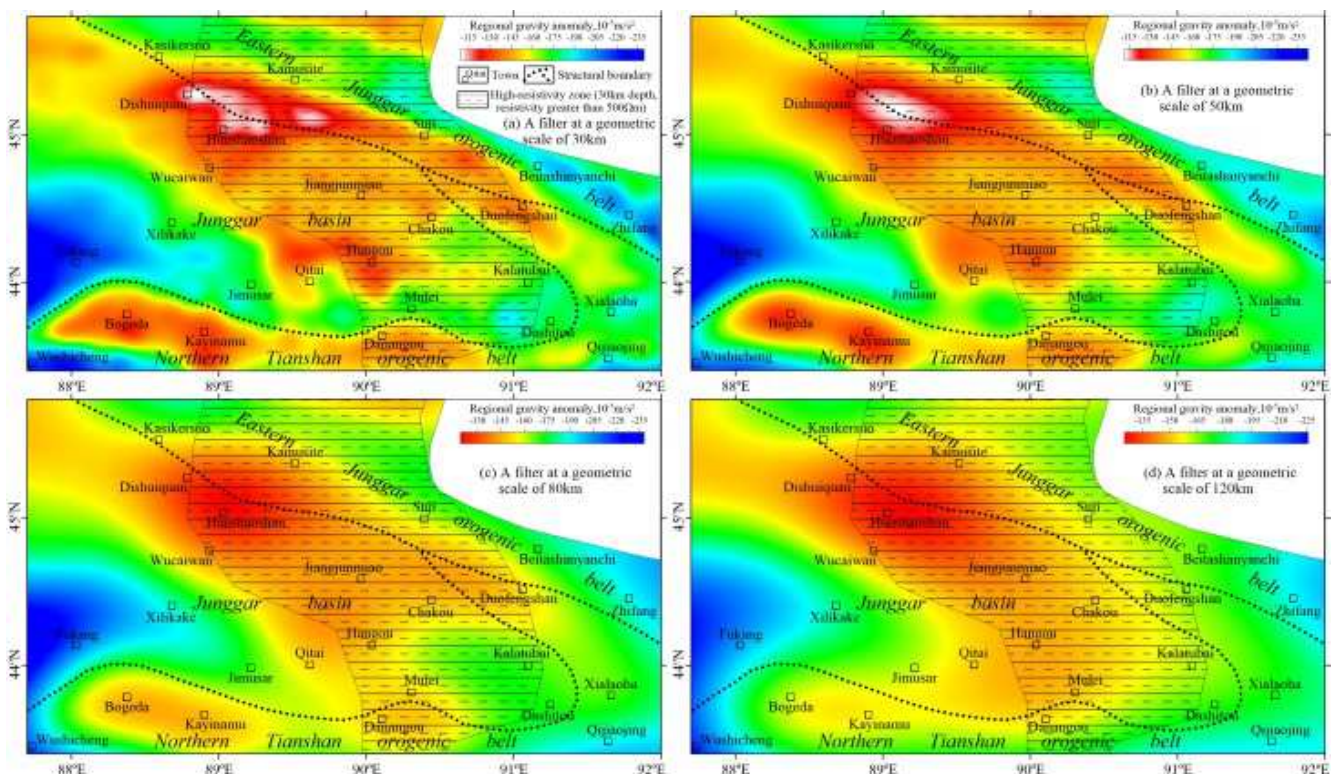

Figure 5. Regional gravity anomaly map of the eastern part of Junggar basin.

3.3. Features and Geological Implication of the Magnetic Anomalies

The RTP aeromagnetic anomaly (Figure 6) shows that the RTP aeromagnetic anomaly is characterized with clear zoning. In the northern Tianshan orogenic belt, the RTP aeromagnetic anomaly displays an EW-trending high-value zone in the west and low-value zone in the east. In the eastern Junggar orogenic belt, the RTP aeromagnetic anomaly displays a NW-trending negative anomaly zone. In the Junggar basin, the RTP aeromagnetic anomaly displays a NWW-trending high-value zone in the north and low-value zone in the south. The

gradient of the RTP aeromagnetic anomaly changes obviously in the northern margin of the Junggar basin, and this gradient zone is consistent with the boundary of these tectonic units, indicating that the gradient zone is caused by the discordogenic fault. There is a NWW-trending high-value zone in the Dishuiquan-Kalatubai area, and this high-value zone consists of seven magnetic highs. The transverse dimension of these magnetic highs is greater than 40 km, and they are located in the West Dishuiquan area, the Wucaiwan area, the Jiangjunmiao area, the Northwest Qitai area, the Chakou area, the North Mulei area, and the West Kalatubai area.
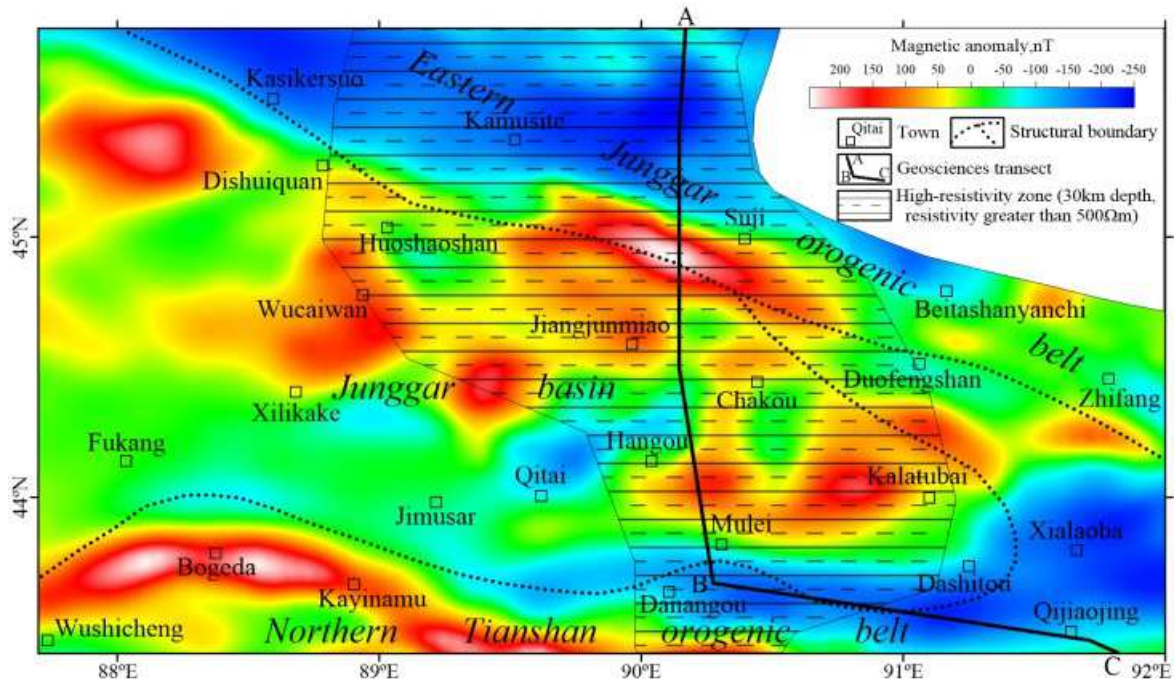
Figure 6. RTP aeromagnetic anomaly map of the eastern part of Junggar basin.
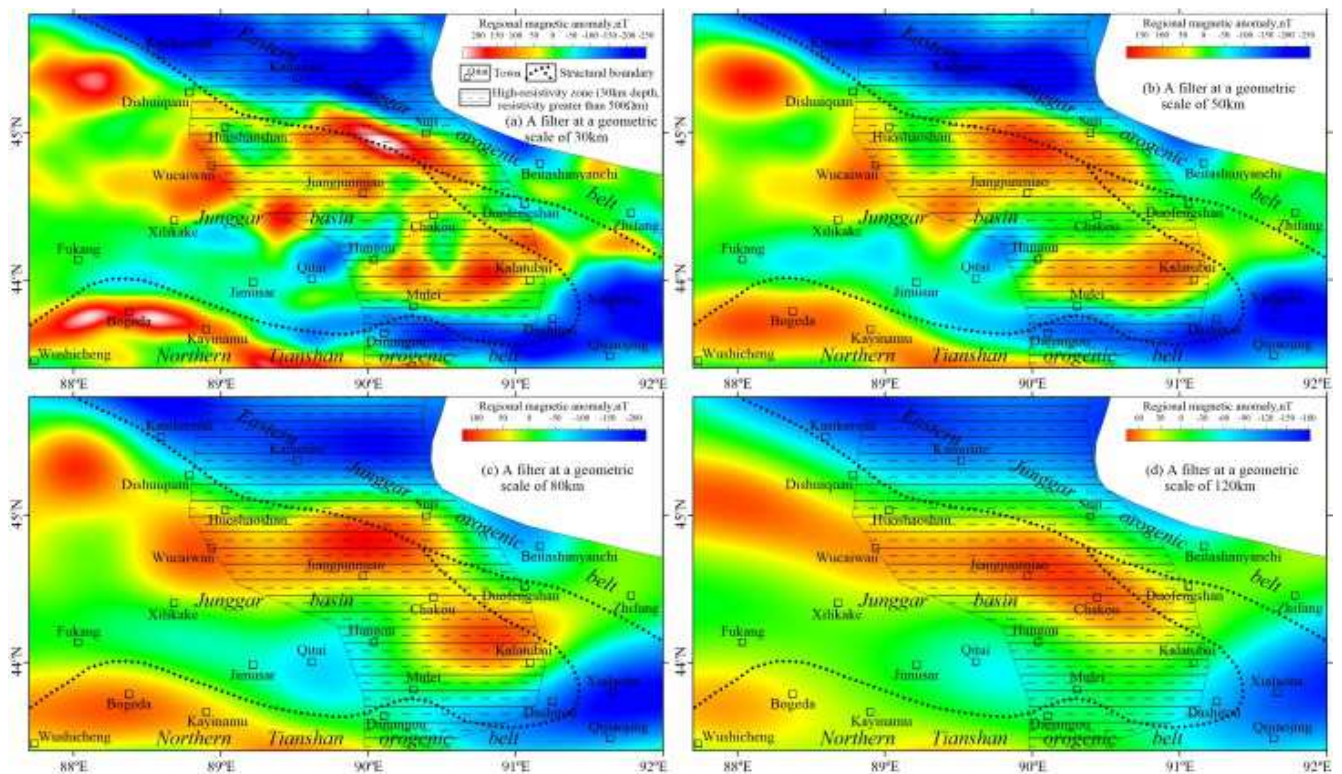

Figure 7. Regional magnetic anomaly map of the eastern part of Junggar basin.

The regional magnetic anomalies are able to reflect the effects of the magnetic field induced by the large scale geological body. Based on the RTP aeromagnetic anomaly data, we extracted the regional magnetic anomalies with multi-filter scales of 30 km, 50 km, 80 km, and 120 km. The regional magnetic anomaly map (Figure 7) shows that the magnetic anomalies with a relatively small scale are suppressed with the filter window length increasing. With the

filter window length increasing, the magnetic high-value zone in the north and the magnetic low-value zone in the south are more and more obvious in the Junggar basin. Especially the regional magnetic anomaly with scale of 120 km, the magnetic high-value zone in the north has even become a NWW-trending magnetic high. These features suggest the deep crustal substance with stronger magnetic property developed in the north of the Junggar basin. With the filter

window length increasing, the position of the magnetic anomaly gradient zone is basically unchangeable in the north side of the Huoshaoshan-Chakou area. These features indicate that the magnetic high zone is controlled by the fault zone of the northern margin of the eastern part of the Junggar basin.

4. Results and Discussion

4.1. Profile Characteristic and Deep Structure

Recently, the wavelet transform method has been widely used in the processing and interpretation of the gravity anomalies and the magnetic anomalies because of its good ability to do multi-scale analysis [35]. Traditional spectrum analysis is usually used to assist wavelet analysis with finding the depth of the gravity anomalies and the magnetic anomalies [36]. Based on the geological background and the estimation of the interfaces depth, we used the wavelet multi-scale

decomposition with 3th/4th/5th order separation to separate the gravity anomalies and the magnetic anomalies in the study area and to examine the deep structural features of the eastern part of Junggar basin. Constraint of the result of the deep seismic sounding, we selected a gravity and magnetic profile for comprehensive interpretation. This profile is coincident with a geoscience transect from Altay to Altun Tagh in the study area [16], the location of the profile shown in Figure 3 and profile interpretation shown in Figure 8. Figure 8a shows that the curves of RTP aeromagnetic anomaly and its 3th~5th order wavelet transform approximation, and Figure 8b shows that the curves of isostatic gravity anomaly and its 3th~5th order wavelet transform approximation, and Figure 8c the curves of Bouguer gravity anomaly and its 3th~5th order wavelet transform approximation, and Figure 8d shows that the elevation curve, and Figure 8e shows that the results of the profile interpretation.
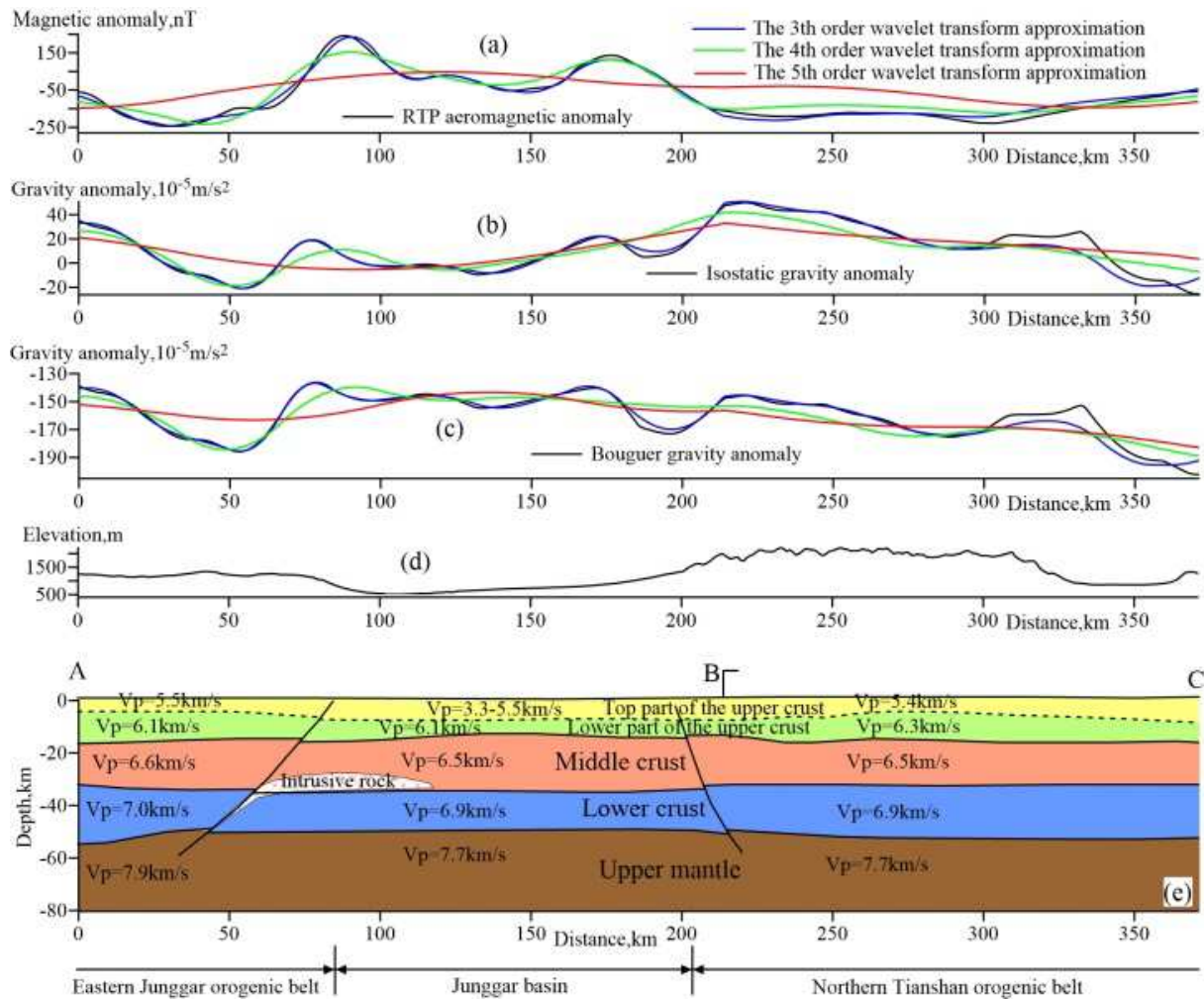
Figure 8. Integrated interpretation of the AC profile. (a) RTP aeromagnetic anomaly and its 3th~5th order wavelet transform approximation; (b) Isostatic gravity anomaly and its 3th~5th order wavelet transform approximation; (c) Bouguer gravity anomaly and its 3th~5th order wavelet transform approximation; (d) Elevation; (e) Crustal and velocity structure (modified after Wang et al. 2004) [16], and the AB section of the AC profile displays NS-trending and the BC section of the AC profile displays NWW-trending.

As shown in Figure 8e, based on the P-wave velocity data of the wide-angle reflection seismic sounding [16], the crust consists of the upper crust, the middle crust, and the lower

crust in the study area. The top part of the upper crust mainly consists of the sedimentary rocks, and its bottom boundary has a larger undulation, and the P-wave velocity of the eastern

Junggar orogenic belt and the northern Tianshan orogenic belt is much greater than that of the Junggar basin. These features suggest that the structure of the top part of the upper crust is complex, and the lateral variation of the material composition is obvious. Therefore, the gravity and magnetic anomalies with a small dimension are easy to form, these anomalies shown in the 50-200 km segment of the Figure 8a, b and c. The lower part of the upper crust is mainly composed of the crystalline material, and the thickness changes obvious. The P-wave velocity of the northern Tianshan orogenic belt is much greater than that of the Junggar basin and the eastern Junggar orogenic belt, indicating that the high-speed substance intruded into the lower part of the upper crust to cause the gravity and magnetic anomalies with a slight larger dimension in the northern Tianshan orogenic belt, these anomalies shown in the 50-250 km segment of the 3 order wavelet transform approximation of the Figure 8a, b, and c. As to the middle crust, the lower crust, and the upper mantle, the P-wave velocity of the Junggar basin and the northern Tianshan orogenic belt is slightly smaller than that of the eastern Junggar orogenic belt, indicating that the lateral density variation of these layers is small and the density of the eastern Junggar orogenic belt is slightly higher than that of the Junggar basin and the northern Tianshan orogenic belt. The thickness of the middle crust changes obvious so as to cause the gravity anomalies and the magnetic anomalies with a larger dimension, these anomalies shown in the 50-250 km segment of the 4 order wavelet transform approximation of the Figure 8a, b, and c. The thickness of the lower crust changes indistinct, and the upper mantle and the lower crust common cause the gravity anomalies and the magnetic anomalies with a large dimension, these anomalies shown in the 50-250 km segment of the 5 order wavelet transform approximation of the Figure 8a, b, and c.

4.2. Deep Geological Implication of the Geophysical Field

Deep crustal resistivity map with 30 km depth shows that the resistivity anomaly is mainly a high-value area in the eastern part of Junggar basin, and there is a good relationship between the high-value areas of the Bouguer gravity anomaly and the resistivity anomalies (Figure 3). These features suggest that the density of the deep crustal substance with 30 km depth is larger and the substance with larger density is one of deep geological factors to cause high gravity anomaly. Compared to the Bouguer gravity anomaly, the changes of the isostatic gravity anomaly are relatively gentle in the eastern part of the Junggar basin. There is also a good relationship between the high-value zones of the isostatic gravity anomaly and the resistivity anomaly, and the relationship is better than between the high-value zones of the Bouguer gravity anomaly and the resistivity anomaly (Figure 4). These features further suggest that the density of the deep crustal substance with 30 km depth is larger and the substance with larger density is one of deep geological factors to cause high gravity anomalies.

The RTP aeromagnetic anomaly map shows that the five magnetic highs are not obvious trend and are nearly equiaxed in the high-value zone of the resistivity at a depth of 30 km (Figure 6). These five magnetic highs are located in the Jiangjunmiao area, the Northwest Qitai area, the Chakou area, the North Mulei area, and the West Kalatubai area. The other two magnetic highs, located in the West Dishuiquan area and the Wucaiwan area, display an EW-trending, and their transverse dimension is larger than that of the five magnetic highs. These features suggest that these magnetic highs are mainly caused by the substance with stronger magnetic property and relatively deeper depth in the eastern part of the Junggar basin.

Based on the regional gravity anomalies, the regional magnetic anomalies and the resistivity anomalies (Figures 5 and 7), it can be seen that the Qitai area appears as gravity high, magnetic low, and resistivity low in the eastern part of the Junggar basin. These features suggest that the intermediate-acidic rocks intruded into the sedimentary rocks of the top part of the upper crust, and the density of the intermediate- acidic rocks is larger than that of the sedimentary rocks, and the magnetic property of the intermediate- acidic rocks is weaker than that of the sedimentary rocks. The scale of the faults in the southern margin and the northern margin of the Junggar basin is relatively large, and there is a significant correspondence between these two boundary faults and the gradient zones of the gravity and magnetic anomalies (Figure 8). These two faults could obviously be used as the passages of the magmatic rocks, so that the mantle substances might surge into the crust. Upwelling of the mantle substances often causes the special geophysical anomalies, such as a high-value zone of gravity anomaly, magnetic anomaly and resistivity anomaly in the north of the eastern part of Junggar basin.

5. Conclusion

The upper mantle uplift and its local fluctuations are relatively small in the eastern part of Junggar basin. The thickness of the upper middle crust changes larger in the northern Tianshan orogenic belt and the eastern Junggar orogenic belt. The lateral variation of the thickness of the middle upper crust is larger in the study area.

The Junggar basin turned down under the northern Tianshan orogenic belt and the eastern Junggar orogenic belt. The mantle substances with larger density and stronger magnetic property and larger resistivity surged into the middle crust along the fault of the northern margin of the Junggar basin, so as to form a high-value zone of gravity anomaly, magnetic anomaly and resistivity anomaly in the north of the eastern part of Junggar basin.

Acknowledgements

References

[1] Kuang, J. (1993). Terrene connection, formation and evolution of Junggar basin. *Xinjiang Petroleum Geology*, 14 (2), 126-132.

[2] Li, J. Y. (2004). Late Neoproterozoic and Paleozoic tectonic framework and evolution of eastern Xinjiang, NW China. *Geological Review*, 50 (3), 304-322.

[3] Xu, Q., Ji, J., Zhao, L., Gong, J., Zhou, J., & He, G., et al. (2013). Tectonic evolution and continental crust growth of Northern Xinjiang in northwestern China: Remnant ocean model. *Earth-Science Reviews*, 126, 178-205.

[4] Zhang, X., Zhao, G., Sun, M., Eizenhofer, P., Han, Y., & Hou, W., et al. (2016). Tectonic evolution from subduction to arc-continent collision of the Junggar ocean: Constraints from U-Pb dating and Hf isotopes of detrital zircons from the North Tianshan belt, NW China. *GSA Bulletin*, 128 (3-4), 644-660.

[5] Zhu, M., Yuan, B., Liang, Z., Yang, D., & Tang, X. (2021). Fault properties and evolution in the periphery of Junggar basin. *ACTA Petrolei Sinica*, 42 (9), 1163-1173.

[6] Zhao, B. (1992). Nature of basement of Junggar basin. *Xinjiang Petroleum Geology*, 13 (2), 95-99.

[7] Li, J. Y., Xiao, X. C., & Chen, W. (2000). Late Ordovician continental basement of the eastern Junggar Basin in Xinjiang, NW China: Evidence from the Laojunmiao metamorphic complex on the northeast basin margin. *Regional Geology of China*, 19 (3), 297-302.

[8] Zhang, J. S., Hong, D. W., & Wang, T. (2004). Geophysical researches on the basement properties of the Junggar basin. *Acta Geoscientica Sinica*, 25 (4), 473-478.

[9] Zhao, J. M., Huang, Y., Ma, Z. J., Shao, X. Z., Cheng, H. G., & Wang, W., et al. (2008). Discussion on the basement structure and property of northern Junggar basin. *Chinese Journal of Geophysics*, 51 (6), 1767-1775.

[10] Yang, F., & Chen, G. (2016). The basement property and evolution of the northern Junggar basin – evidence from zircon U-Pb chronology and trace element. *Arabian Journal of Geosciences*, 9, 353-368.

[11] Li, J. Y., & Xu, X. (2004). Major problems on geologic structures and metallogenesis of northern Xinjiang, northwest China. *Xinjiang Geology*, 22 (2), 119-124.

[12] Li, J. Y., He, G. Q., Xu, X., Li, H. Q., Sun, G. H., & Yang, T. N., et al. (2006). Crustal tectonic framework of northern Xinjiang and adjacent regions and its formation. *Acta Geologica Sinica*, 80 (1), 148-168.

[13] Li, Q., Liu, R. F., Du, A. L., & Yang, M. L. (1994). Seismic tomography of Xinjiang and adjacent region. *Acta Geophysica Sinica*, 37 (3), 311-320.

[14] Xu, G. M., Yao, H. J., Zhu, L. B., & Shen, Y. S. (2007). Shear wave velocity structure of the crust and upper mantle in western China and its adjacent area. *Chinese Journal of Geophysics*, 50 (1), 193-208.

[15] Wang, Z. H., Liu, J., Zhou, L. Q., & Wang, H. T. (2008). Tomography of 3D velocity in earth's crust and upper mantle of middle Tianshan. *Inland Earthquake*, 22 (3), 203-211.

[16] Wang, Y. X., Han, G. H., Jiang, M., & Yuan, X. C. (2004). Crustal structure along the geosciences transect from Altay to Altun Tagh. *Chinese Journal of Geophysics*, 47 (2): 240-249.

[17] Li, Y., Yu, Y., Shen, J., Shao, B., Qi, G., & Deng, M. (2016). Active faults and seismogenic models for the Urumqi city, Xinjiang autonomous region, China. *Earthquake Science*, 29 (3), 173-184.

[18] Zhao, J. M., Li, Z. C., Cheng, H. G., Yao, C. L., & Li, Y. (2004). Structure of lithospheric density and geomagnetism beneath the Tianshan orogenic belt and their geodynamic implications. *Chinese Journal of Geophysics*, 47 (6), 8-17.

[19] Zhang, C., Dong, Y., Yuan, B., & Li, Y. (2014). A genesis analysis of the regional gravity and magnetic anomalies in the northern part of eastern Xinjiang, Northwest China. *Petroleum Science and Technology*, 32, 2075-2085.

[20] Deng, Y., Levandowski, W., & Kusky, T. (2017). Lithospheric density structure beneath the Tarim basin and surroundings, northwestern China, from the joint inversion of gravity and topography. *Earth and Planetary Science Letters*, 460, 244-254.

[21] Zhu, X., Wang, T., Huang, H., & Zheng, H. (2022). An aeromagnetic study of fault structures underneath the region across the Chinese Altai orogen, Junggar Basin, Tianshan orogen, and Tarim Basin. *Journal of Asian Earth Sciences*, 239, 105418.

[22] Gao, G., Kang, G., Bai, C., & Li, G. (2013). Distribution of the crustal magnetic anomaly and geological structure in Xinjiang, China. *Journal of Asian Earth Sciences*, 77, 12-20.

[23] Yuan, X. C. (2005). 3D lithospheric structure of western China and its enlightenment on petroleum prospecting. *Geology in China*, 32 (1), 1-12.

[24] Yuan, X. C. (2007). Sandwich lithospheric structure of Xinjiang and its relation to petroleum resources. *Geology in China*, 34 (1), 1-7.

[25] Li, L. (1996). The geoelectrical characteristic of crust and upper mantle in the continental region of China. *Acta Geophysica Sinica*, 39 (Supp.), 130-140.

[26] Xu, Y., Yang, B., Zhang, S., Liu, Y., Zhu, L., & Huang, R., et al. (2016). Magnetotelluric imaging of a fossil Paleozoic intraoceanic subduction zone in western Junggar, NW China. *Journal of Geophysical Research: Solid Earth*, 121, 4103-4117.

[27] Zhang, S., Xu, Y., Jiang, L., Yang, B., Liu, Y., & Griffin, W., et al. (2017). Electrical structures in the northwest margin of the Junggar basin: Implications for its late Paleozoic geodynamics. *Tectonophysics*, 717, 473-483.

[28] Becker, J. J., Sandwell, D. T., Smith, W. H. F., Braud, J., Binder, B., & Depner, J. (2009). Global bathymetry and elevation data at 30 arc seconds resolution: SRTM30_PLUS. *Marine Geodesy*, 32 (4), 355-371.

[29] Zhang, X., Zhao, G., Eizenhofer, P., Sun, M., Han, Y., & Hou, W. (2016). Late Ordovician adakitic rocks in the Central Tianshan block, NW China: Partial melting of lower continental arc during back-arc basin opening. *GSA Bulletin*, 128 (9-10), 1367-1382.

[30] Li, Y. P., Li, J. Y., Sun, G. H., Zhu, Z. X., & Yang, Z. Q. (2007). Beaement of Junggar basin: evidence from detrital zircons in sandstone of previous Devonian Kalamaili formation. *Acta Petrologica Sinica*, 23 (7), 1577-1590.

[31] Xu, P., Fu, R. S., Huang, J. P., Dai, Z. Y., & Zha, X. J. (2005). Correction to the Moho discontinuity depth of the northwestern China using the data of seismologic tomography. *Acta Seismologica Sinica*, 27 (6), 598-604.

[32] Xiong, X. S., Gao, R., Li, Q. S., Wang, H. Y., & Hou, H. S. (2010). The Moho depth of northwest China revealed by seismic detection. *Acta Geoscientica Sinica*, 31 (1), 23-31.

[33] Yuan, B. Q., Xie, W. S., Liu, G. H., & Zhang, C. G. (2012). Gravity field and tectonic features of Block L2 in the Lamu basin, Kenya. *Geophysical Prospecting*, 60, 161-178.

[34] Yuan, B. Q., Song, L. J., Han, L., An, S. L., & Zhang, C. G. (2018). Gravity and magnetic field characteristics and hydrocarbon prospects of the Tobago basin. *Geophysical Prospecting*, 66, 1586-1601.

[35] Li, C. B., Wang, L. S., Sun, B., Feng, R. H., & Wu, Y. J. (2015). Interpretations of gravity and magnetic anomalies in the Songliao basin with wavelet multi-scale decomposition. *Frontiers of Earth Science*, 9 (3), 427-436.

[36] Albora, A. M., & Ucan, O. N. (2001). Gravity anomaly separation using 2-D wavelet approach and average depth calculation. *Dogus University Journal*, 3, 1-12.